SUPPORTING INFORMATION -

Consequences of Overtones in Raman Spectra for Structural Assignment of Nickel Anodes during Alkaline Electrolysis

[1]

Justus Leist, Annika Neufischer, Timo Jacob,* and Albert K. Engstfeld*

Institute of Electrochemistry, Ulm University, D-89069 Ulm, Germany

E-mail: timo.jacob@uni-ulm.de; albert.engstfeld@uni-ulm.de

Contents

S1 Materials preparation

$HClO_4$ (99.999%), $Ni(NO_3)_2$ (99.999%), KCl (EMSURE), KOH (99.99 % semiconductor grade) and $LiOH \cdot H_2O$ (99.995%) were purchased from Sigma Aldrich. Solutions and electrolytes were prepared with Milli-Q water (18.2 MΩ), except for experiments with isotope-labeled water, i.e., D_2O (99.9 %) and $H_2{}^{18}O$ (97 %), which were purchased from Deutero. Caro's acid was prepared with 3 parts of 95 % H_2SO_4 (technical grade) from VWR chemicals and 1 part of 30 % H_2O_2 (for synthesis) from Sigma-Aldrich. Possible Fe impurities in KOH were removed according to the procedure described by Trotochaud et al.[1] This procedure involved precipitating $Ni(NO_3)_2$ in 1 M KOH. The precipitated $Ni(OH)_2$ was washed with Milli-Q water and centrifuged. Afterwards, KOH was added to the redispersed $Ni(OH)_2$ and shaken. After a resting period of at least 3 h, the KOH mixture was centrifuged and subsequently used for measurement. All perfluoroalkoxy alkane (PFA, filament bought from filamentworld), polyvinylidene fluoride (PVDF, filament bought from 3Dogg), and glass components were cleaned by soaking in Caro's acid for at least one day. Before the experiments, the components were rinsed with and subsequently boiled in ultrapure water at least three times for at least one hour.

S2 Raman spectroscopy measurement cell

In situ Surface enhanced Raman spectroscopy measurements were performed in a PFA cell (VITLAB GmbH) with a 3D printed lid made of PVDF, which is illustrated in Fig. S1. The lid contained a hole covered by a transparent borosilicate glass disc (Marienfeld), allowing the laser of the Raman spectrometer to interact with the sample. The glass disc was mounted shortly before the start of the experiment to minimize its dissolution in alkaline electrolytes, leading to silicate contamination. A magnetic stirring bar was included to disperse the bubbles formed during the OER, which limit the Raman measurements at high overpotentials. For measurements in isotope-labeled water (KOD and $K^{18}OH$), a similar cell was used, but with a smaller electrolyte volume and without a stirring bar. The stirring bar was used only during measurements in the larger cell under OER conditions, as no effect was observed under other conditions, and omitting it ensured consistency between measurements performed in the larger and smaller cells.

The potential was controlled with a PG-285 (HEKA-Elektronik) Potentiostat, using a leakless Ag/AgCl miniature reference electrode (eDAQ) and a Pt wire (MaTeck, 99.99 %) as a counter electrode. The Pt wire was prepared by soaking in hot acetone (50 °C) for at least half an hour and subsequent sonication in Milli-Q water at room temperature for another hour. The Raman spectra were recorded with a Confocal Raman microscope inVia (Renishaw) equipped with a CCD detector, a He/Ne laser with a wavelength of 633 nm (maximum power of 17 mW), and a 50× long working distance objective.

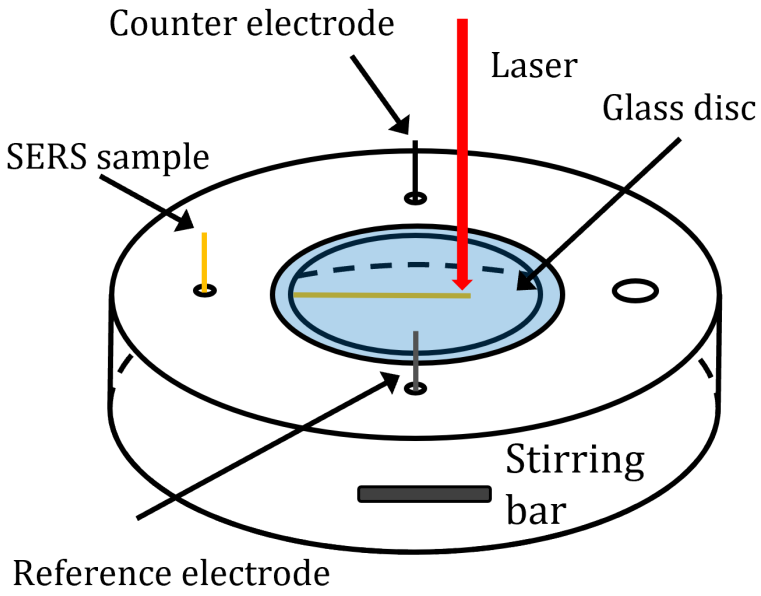

Figure S1: Schematic illustration of the *in situ* SERS cell, containing a Ag/AgCl reference, a Pt counter electrode and the SERS sample as working electrode. In the middle of the cell, an opening for the Laser is covered with a glass disc to prevent bulging of the electrolyte. A stirrer is added to deal with bubble formation and pH shift at high applied potentials during the OER.

S3 Sample preparation

The SERS active Ni working electrode (Ni supported on a Au substrate) was prepared electrochemically in a glass cell, equipped with a Ag/AgCl (3.4 M) reference electrode and a graphite rod counter electrode. The potential of the working electrode was controlled with a VSP-300 potentiostat from BioLogic. The preparation procedure for the working electrode was adapted from the procedures presented by Diaz-Morales et al.[2,3] First, a Au wire (MaTecK 99.995 %) was annealed in a butane flame. The wire was then dipped 2 cm into a 0.1 M KCl electrolyte and roughened by 30 potential cycles between −0 3 and 1.2 V vs. 3.4 MAg/AgCl, recorded at a scanrate of 500 mV s^{-1}. The last cycle of this procedure is shown in Fig. S2. During the scans, the potential was held at the upper potential limit for 1.3 s and at the lower limit for 30 s.[3] A cyclic voltammogram 0.1 M $HClO_4$ before and

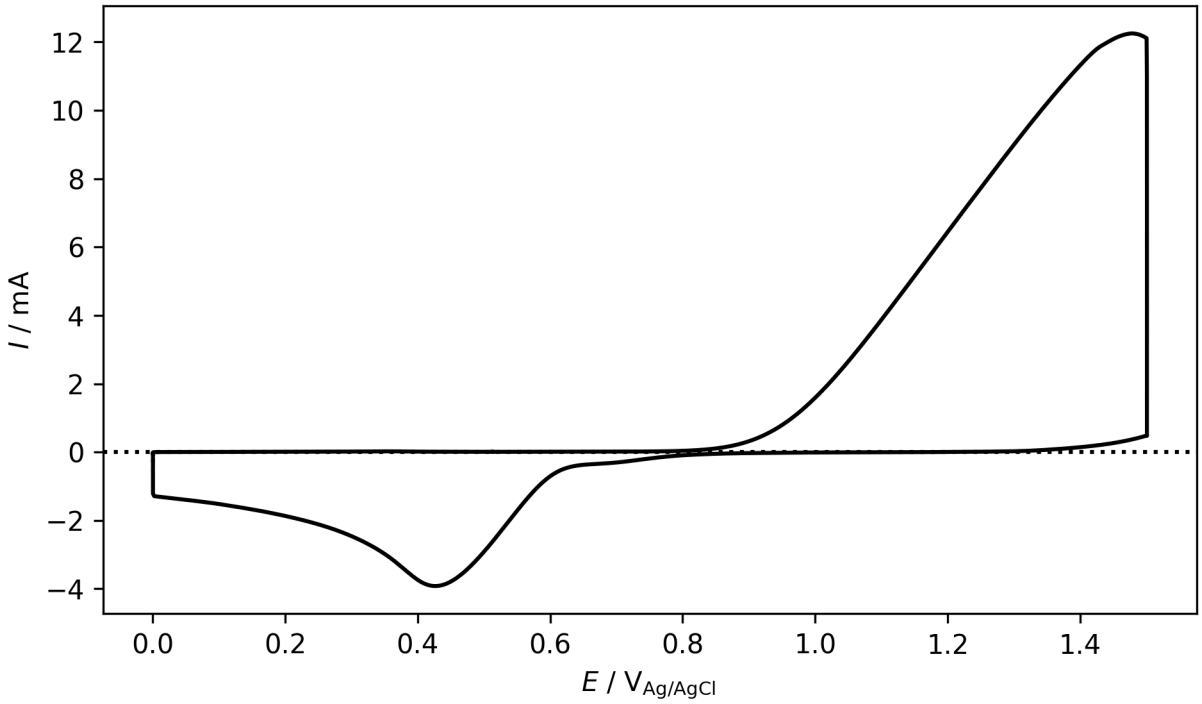

Figure S2: Electrochemical procedure for the roughening of a Au wire in 0.1 M KCl, showing in this case the last out of 30 cycles, recorded at a scanrate of 500 mV s^{-1}. At the upper / lower potential limit the potential was held for 1.3 s / 30 s.

after the roughening in KCl is shown in Fig. S3. For this, 1 cm of the Au wire was dipped into the solution, which was purged with nitrogen for 10 min and cycles were recorded at a scanrate of 5 mV s^{-1} vs Ag/AgCl (3.4 M). Afterwards, the surface area of the Au wire was determined by the reduction peak in the cyclic voltammogram recorded in 0.1 M $HClO_4$ after the roughening. By integrating the reduction peak in the negative going scan and correcting for the capacitive current of the double layer, the surface area can be calculated assuming a charge of 390 µC cm^{-2}.[2] Here, a surface area of 0.34 cm^2 was calculated.

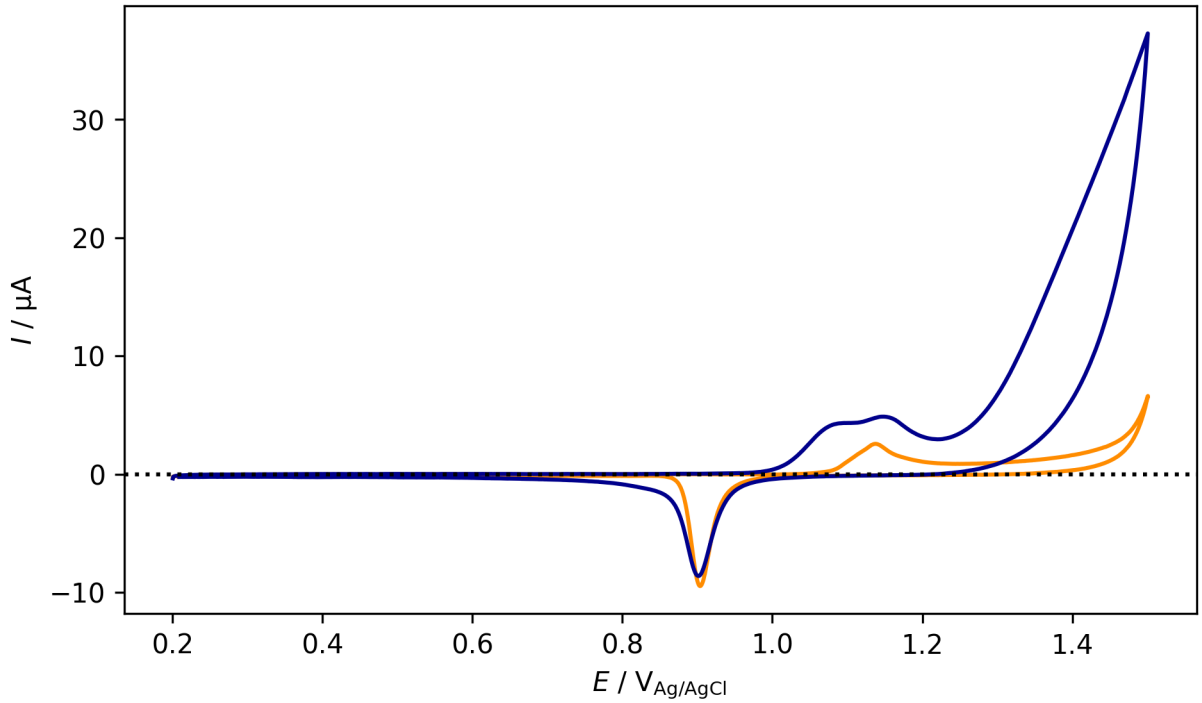

Figure S3: Cyclic voltammogram for a Au wire recorded in 0.1 M $HClO_4$ at a scan rate of 5 mV s^{-1}, before (orange) and after (blue) electrochemical roughening (see text for details).

The deposition of Ni was performed by immersing 1 cm of the Au wire into a mixed 5 mM $Ni(NO_3)_2$ and 0.1 M $KClO_4$ solution. A current of 10 µA was applied between the Au working electrode and a graphite counter electrode.

To ensure a sufficiently thick Ni coating and prevent AuO artifacts in the SER spectra,[4] the deposition time was adjusted to produce roughly 75 layers on the Au wire. The required time was calculated using the surface area of the Au wire assuming a charge of 726 µA cm^{-2}

per layer as described elsewhere.[2]

The quality of the deposited Ni film was determined from cyclic voltammetry and *in situ* Raman spectroscopy measurements. The cyclic voltammogram recorded in 0.1 M KOH (stirred electrolyte), at a scanrate of $5\,\mathrm{mV\,s^{-1}}$ is shown in Fig. S4, shows typical features for Ni electrodes in a KOH electrolyte (see manuscript for further details). For incomplete Ni films, additional features are observed that are related to the Au substrate.

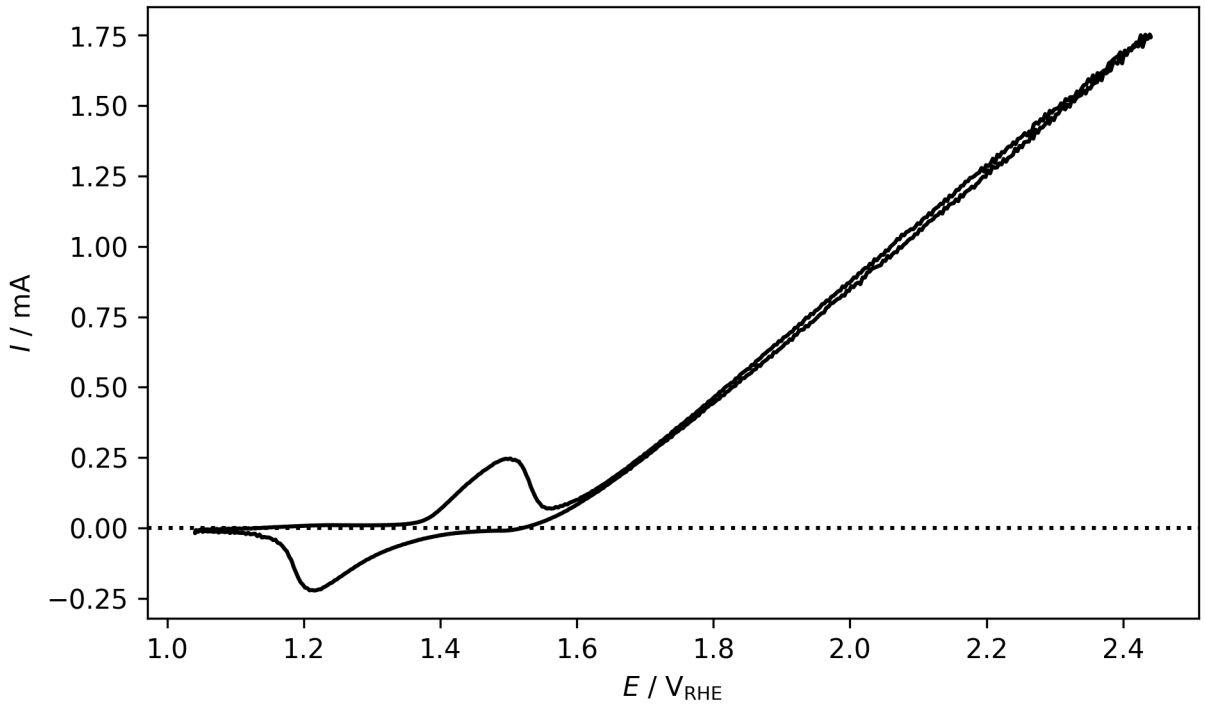

Figure S4: CV of Ni deposited Au wire measured in a stirred 0.01 M KOH with a scanrate of $5\,\mathrm{mV\,s^{-1}}$ and limits of $1.04\,\mathrm{V_{RHE}}$ and $2.44\,\mathrm{V_{RHE}}$.

Raman spectra showing a successful deposition are shown in Fig. S6. Up to $1.34\,\mathrm{V_{RHE}}$, the SER spectra correspond to that of $Ni(OH)_2$. A broad band at $550\,\mathrm{cm^{-1}}$ belonging to AuO_x can not be detected.[4] At $1.39\,\mathrm{V_{RHE}}$, initial formation of NiOOH is visible, as peaks at 480 and $560\,\mathrm{cm^{-1}}$ begin to form. At $1.44\,\mathrm{V_{RHE}}$ only NiOOH is visible. Additionally, the Raman spectra of the SERS sample can be compared to a Raman spectrum recorded with a pure Ni sheet (Mateck, 99.99 %) in 0.01 M KOH collected at $1.5\,\mathrm{V_{RHE}}$ (Fig. S5). However, due to the lack of the surface enhancement effect of the Au wire, the total intensity and thus

quality of the spectrum is lowered by a factor of around seven. Still, Raman spectroscopy of NiOOH without surface enhancement is possible.[4] In contrast, detecting Raman signals of $Ni(OH)_2$ without surface-enhancement under operating conditions is challenging.

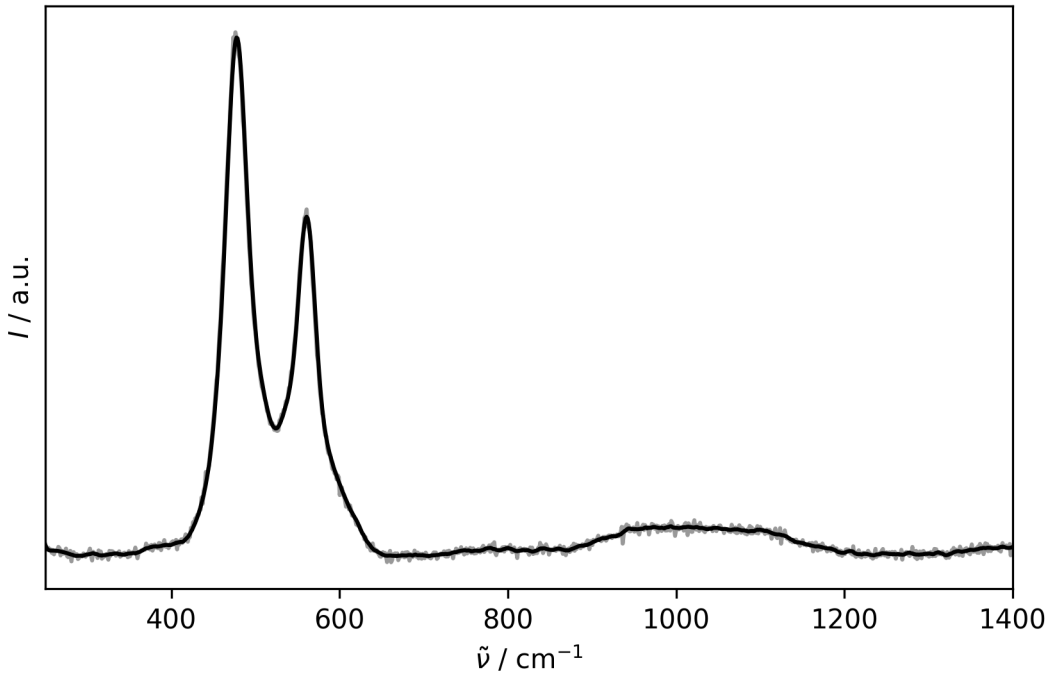

Figure S5: Raman spectrum of Ni sheet in 0.01 M KOH measured with an applied potential of 1.5 V_{RHE}.

S4 Raman spectra processing

The raw Raman spectra were post-processed by adjusting the baseline and removing noise. The baseline was determined with an asymmetric least square smoothing[5] and subtracted from the signal. Additionally, a Savitzky-Golay filter was applied to all spectra to remove noise,[6] which improves the visual separation of peaks from the noise.

Measurements performed during different measuring series and during OER conditions can have varying total intensity. To improve comparability, the intensity of each NiOOH spectrum in the main manuscript was scaled so that the maximum of the first peak at 450 to 480 cm^{-1} of each spectrum is set to the same intensity. Peak deconvolution of various SER spectra was performed using the Voigt model from the Python-based lmfit library.[7] To deconvolute overtone and fundamental modes, their positions were estimated by summing the corresponding fundamental frequencies. A tolerance of ± 10 cm^{-1} was allowed to account for possible deviations during the deconvolution process.

S5 SER spectra of $Ni(OH)_2$ oxidation to NiOOH

The transition of $Ni(OH)_2$ to NiOOH can be monitored by Raman spectroscopy, as shown in Fig. S6, including an intermediate stage in which peaks corresponding to both phases are observed in the same spectrum.

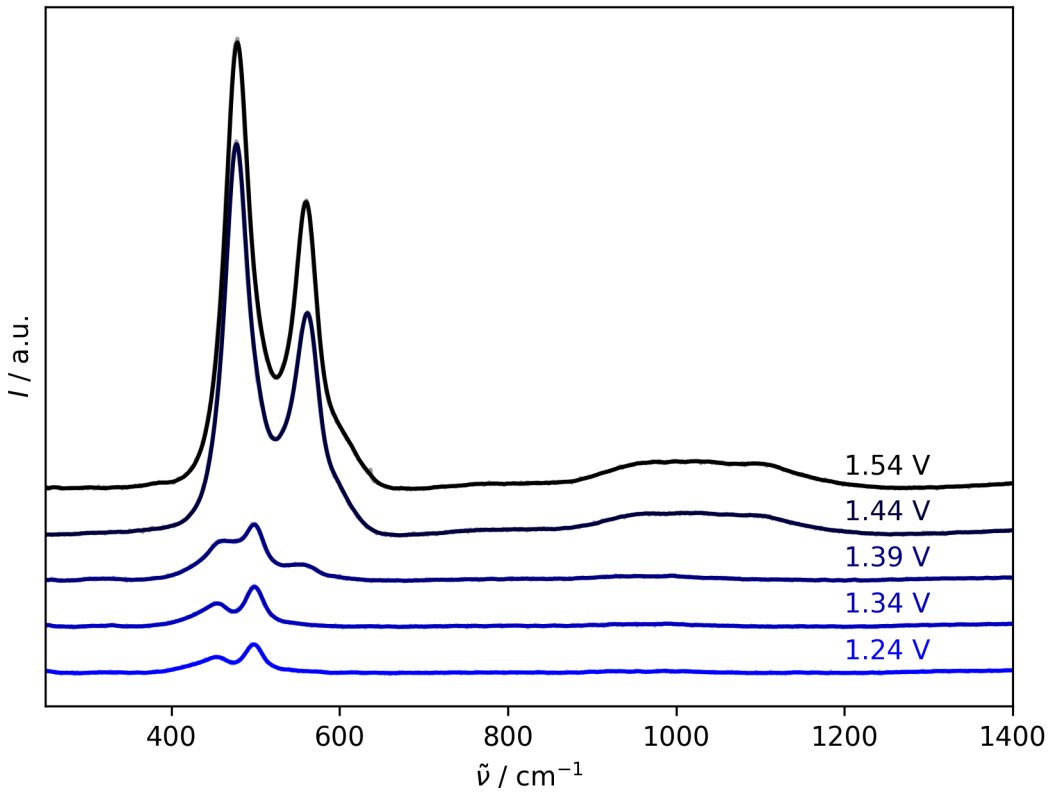

Figure S6: SER spectra of Ni deposited Au wire in 0.01 M KOH at potentials from 1.24 V_{RHE} to 1.54 V_{RHE}. No normalization was performed for the here recorded spectra. The transition from $Ni(OH)_2$ to NiOOH is apparent at about 1.39 V.

S6 SER spectra of $Ni(OH)_2$ in isotope labeled electrolyte

Isotope-labeled electrolytes, such as KOD and $K^{18}OH$, were used to investigate the lattice composition of $Ni(OH)_2$. Distinct Raman shifts confirm the presence of hydrogen and oxygen within the lattice as shown in Fig. S7. The peak positions of the spectra in Fig. S7 are listed in Tab. S1.

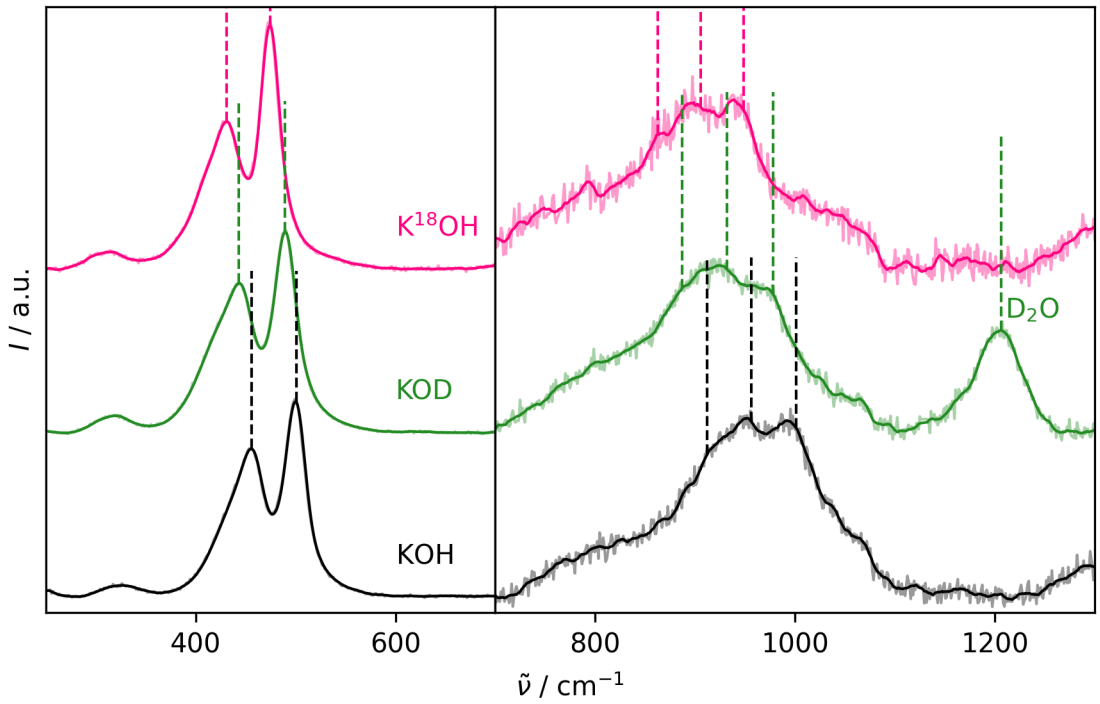

Figure S7: SER spectra of $Ni(OH)_2$ in 0.01 M KOH, KOD and $K^{18}OH$ at an electrode potential of 1.14 V_{RHE}. The position of the fundamental modes and the corresponding overtone and combination modes are highlighted as well as the D_2O bending vibration at 1205 cm^{-1}.

Table S1: Position of fundamental modes of SER spectra of $Ni(OH)_2$ in 0.01 M KOH, KOD and $K^{18}OH$ (inferred from Fig. S7) at an applied potential of 1.1 V_{RHE}.

Electrolyte	$\tilde{\nu}(E_g$ or $A_{1g})/cm^{-1}$	$\tilde{\nu}(E_g$ or $A_{1g})/cm^{-1}$
KOH	455.8	500.6
KOD	443.3	489.4
$K^{18}OH$	431.0	473.7

S7 SER peak position of Raman active modes of NiOOH in various electrolytes

Table S2: Position of fundamental modes in SER spectra of NiOOH recorded in 0.01 M KOH, LiOH, $KClO_4$, KOD and $K^{18}OH$ at an electrode potential of 1.5 V_{RHE}. Corresponding SER spectra are shown in Fig. 2 in the manuscript.

Electrolyte	$\tilde{\nu}(E_g)/cm^{-1}$	$\tilde{\nu}(A_{1g})/cm^{-1}$
KOH	478.6	558.2
LiOH	478.7	558.3
$KClO_4$	477.3	555.7
KOD	477.5	555.9
$K^{18}OH$	453.6	526.1

S8 Deconvolution of SER spectrum of NiOOH in KOD

The SER spectrum of NiOOH in KOD can be deconvoluted in the same manner as the spectra in KOH and $K^{18}OH$ as shown in Fig. S8. The deconvoluted spectrum recorded in KOD exhibits a similar trend compared to that in KOH, except for a shift of the D_2O bending vibration, which is consistent with the assumption that NiO_2 is present instead of NiOOH.

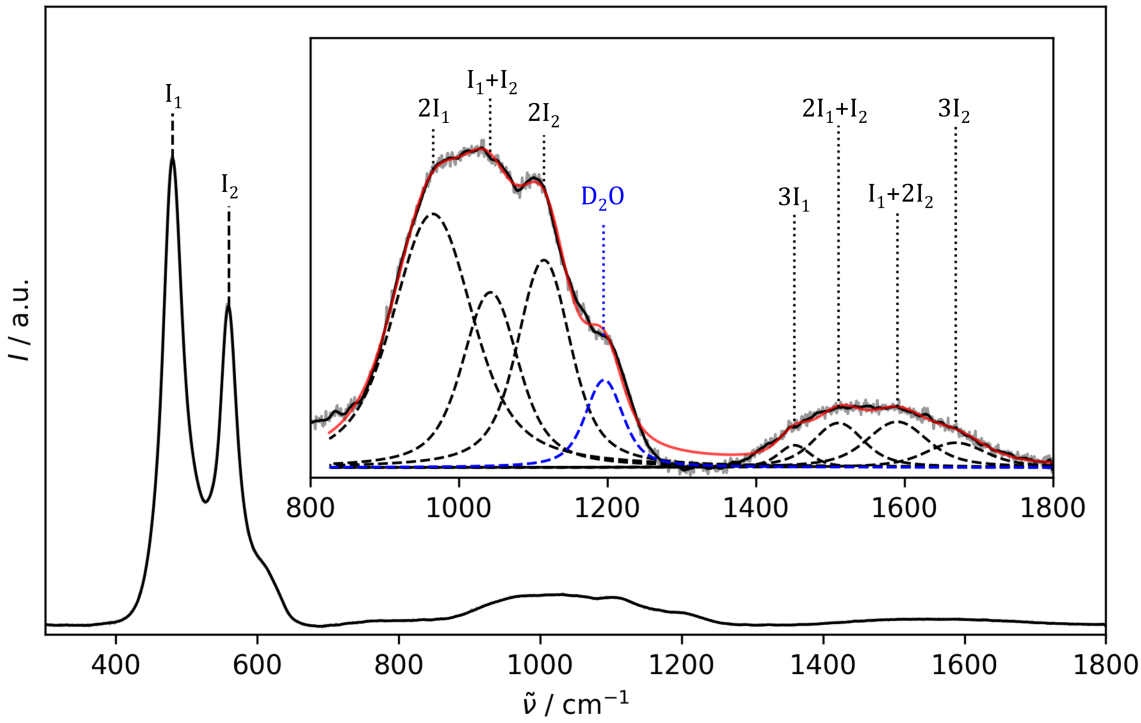

Figure S8: *In situ* SER spectra for Ni in 0.01 M KOD, recorded at electrode potentials of 1.64 V at which NiOOD/NiO_2 is formed. The inset magnifies the region between 800 cm^{-1} and 1800 cm^{-1} by a factor of 15 and highlights the first and second overtone and combination band. Additionally, the bands in the inset were deconvoluted using the position of the overtone and combination modes and are highlighted. The bending mode of D_2O was accounted for in the deconvolution as well and is highlighted in blue. The peak positions are summarized in Tab. 1 in the main manuscript.

S9 Computational method

DFT calculations were performed with the Vienna *Ab initio* Simulation Package (VASP) 6.2.0.[8,9] Projector augmented wave (PAW) was utilized to describe electron-core interactions.[10] Spin-polarized calculations were performed assuming ferromagnetic coupling and a high-spin electronic configuration for the nickel ions. The generalized gradient approximation (GGA) developed by Perdew, Burke, and Ernzerhof (PBE) was employed to describe electronic exchange and correlation.[11] The calculations were performed without Hubbard U correction since the NiOOH geometry is not affected by this correction.[12] Furthermore, DFT-D3 correction was employed to correct for dispersion interactions.[13]

In total, four structures were created (see Fig. 3 in the manuscript), including two bulk structures and two slabs, which were computed with a $5 \times 3 \times 4$ and a $8 \times 4 \times 1$ k-point mesh according to the Monkhorst-Pack scheme, respectively.[14] Plane waves with a cutoff of 500 eV and 600 eV for the bulk and slab structures were employed, respectively, and Gaussian smearing with a width of 0.05 eV was used. Convergence was achieved when the maximum force applied on any atom is smaller than 0.05 meV/Å and the energy difference of the electronic self-consistent field (SCF) was smaller than 10^{-6} eV.

For calculating the β-NiOOH bulk structure, we assume the layered Brucite type structure similar to that of $Ni(OH)_2$, but with half of the hydrogen atoms removed, consistent with previous studies.[15,16] The employed unit cell contains two formula units NiOOH. For the eight atoms, a monoclinic unit cell with lattice parameters of $a = 2.92$ Å, $b = 5.92$ Å, $c = 4.80$ Å, $\alpha = 88.4°, \beta = 71.7°, \gamma = 119.7°$ was used.

Next, a β-NiOOH surface was created using four layers of the optimized β-NiOOH. Each layer consisted of four formula units of NiOOH and the position of the bottom two layers were fixed. To capture the influence of the surface on the Raman spectra, vacuum was added on top of the surface by increasing c by 14.4 Å.

Bulk NiO_2 was created by removing the H in the NiOOH unit cell and optimizing its

geometry. The unit cell contains 6 atoms and has the lattice parameter $a = 2.82\,\text{Å}, b = 5.64\,\text{Å}, c = 5.03\,\text{Å}, \alpha = 76.8°, \beta = 73.3°, \gamma = 120.0°$. Finally, based on the NiO_2 structure, a slab with four layers and a (0001) surface was created. The two bottom layers were fixed in their bulk geometry. Additionally, 15.1 Å was added to c to simulate vacuum on top of the slab.

Phonons were calculated for all structures with a finite difference approach with a step size of 0.015 Å and a cutoff of 600 eV for the plane wave energy. To calculate the phonons for the NiOOH and NiO_2 surfaces, the position of the bottom three layers was fixed, and only modes for the top layer were calculated. Finally, to calculate Raman intensities, an adapted Python script by Fornari and Stauffer was employed, which allows calculating the macroscopic dielectric tensor with respect to each normal mode by displacing each atom by 0.01 Å along each normal mode vector.[17] Again, for the NiOOH and NiO_2 slabs, only atoms at the top layer were displaced. Raman intensities were then calculated according to the procedure proposed by Porezag et al.[18]

The complete calculated Raman spectra for the bulk structures of NiOOH and NiO_2 are shown in Fig. S9. Furthermore, the intensity of all calculated phonons and their positions are summarized for each structure in Tab. S4 (NiO_2 bulk), S5 (NiO_2 surface), S6 (NiOOH bulk) and S8 (NiOOH surface).

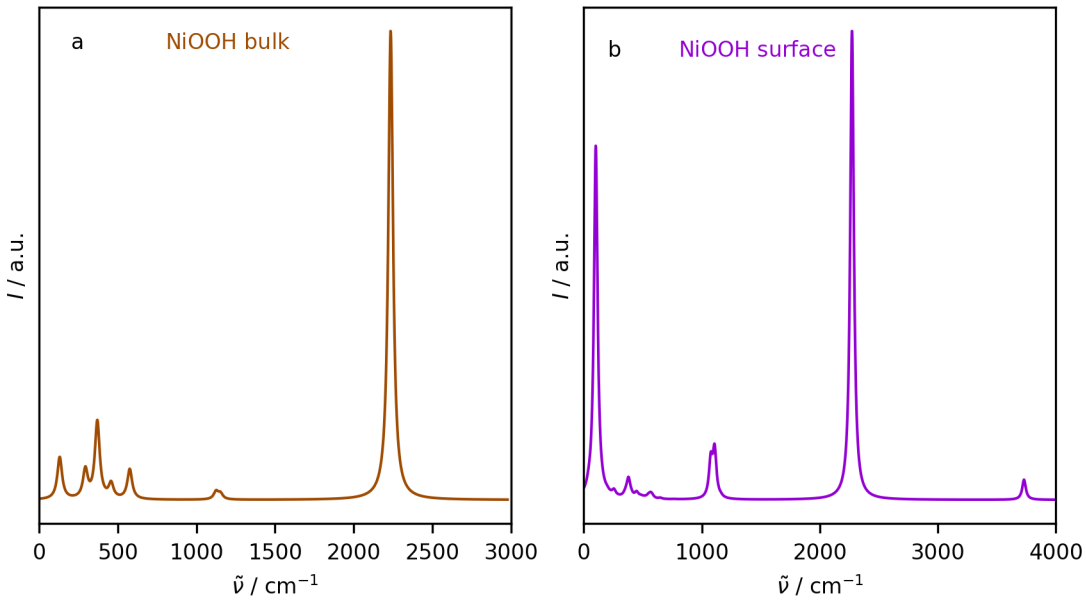

Figure S9: Complementary complete predicted Raman spectrum for the NiOOH bulk (a) and surface (b), to that in Fig. 4 in the manuscript. Calculated spectra are displayed using an arbitrary Lorentzian peak width for comparison with experimental data.

Table S3: Optimized lattice parameters of NiOOH reported in recent literature. Parameters have been rescaled to correspond to one formula unit of NiOOH. Original values are provided in brackets.

Structure	Method	a, b, c [Å]	α, β, γ [°]
my work	DFT + D3	2.918, 2.9605, 4.797	88.38, 71.74, 119.68
LL[19]	DFT+U (5.5)	2.416 (4.922), 2.798 (11.193), 4.817	90.00, 89.93, 75.96
MC1[16]	DFT+U (5.5) (PBE)	2.945 (5.893), 2.993 (5.986), 4.719 (9.439)	120.56, 80.22, 87.35
MC2[16]	DFT+U (5.5)	2.94, 2.992 (5.984), 5.004	120.56, 89.41, 70.34
TC[20]	DFT+U	2.926, 2.957 (5.913), 4.839	80.0, 90.0, 119.7
ZC1[12]	DFT	2.59 (5.18), 2.93, 4.509	90.01, 101.89, 90.00
ZC2[12]	DFT+U (5.5)	2.579 (5.157), 2.898, 4.669	90.175, 101.926, 90.104
EE[21]	DFT+U (5.5)	2.92, 2.92, 5.01	70, 110, 120
HE[22]	DFT+U (5)	2.91 (5.82), 2.92 (11.69), 4.88 (9.77)	119.03, 69.66, 109.79
C1[23]	optB88-vdW+U (5.3)	2.64 (5.288), 2.829, 4.536	90, 103.54, 90
C2[23]	optB88-vdW+U (5.3)	2.65 (5.296), 2.828, 4.576	90, 75.64, 90
HL1[24]	DFT+U (5.5) +D3	2.271 (9.085), 2.956 (5.913), 5.023	90, 90, 96.66
HL2[24]	DFT+U (5.5) +D3	2.499 (4.997), 2.994 (5.989), 4.510 (9.019)	93.73, 76.68, 97.94
HL3[24]	DFT+U (5.5) +D3	2.315 (9.259), 2.922 (5.844), 5.086	90, 90, 77.57
HL4[24]	DFT+U (5.5) +D3	2.571 (5.142), 2.899 (5.789), 4.633 (9.266)	90, 90, 101.9

Table S4: Calculated vibrational modes of the NiO_2 bulk slab (Fig. 4 in the manuscript) without the acoustical modes. Known symmetries derived from group theory analysis are given.

mode	$\tilde{\nu}$ [cm^{-1}]	activity [a.u.]	symmetry
01	626.98	2.55	A_{2u}
02	613.04	1.97	
03	568.03	0.47	
04	567.54	0.18	
05	557.68	7947.43	A_{1g}
06	550.82	0.95	E_u
07	547.94	0.28	E_u
08	541.57	0.05	
09	479.49	3998.57	E_g
10	477.25	2437.91	E_g
11	449.85	0.66	
12	437.04	1.04	
13	423.92	2.28	
14	289.4	0.00	
15	230.00	0.133	

Table S5: Calculated vibrational modes and their predicted intensities of the NiO_2 surface slab (Fig. 4 in the manuscript). Known symmetries derived from group theory analysis are given.

mode	$\tilde{\nu}$ [cm^{-1}]	activity [a.u.]	symmetry
01	633.68	33.93	A_{2u}
02	608.58	1.57	
03	608.37	1.33	
04	608.29	0.24	
05	568.12	1.50	
06	567.33	0.54	
07	566.81	0.16	
08	560.45	0.54	
09	559.14	2.12	
10	558.81	57.70	
11	556.66	1088.41	A_g
12	552.54	423.37	E_u
13	550.84	122.30	E_u
14	547.79	0.86	
15	547.53	0.81	
16	545.82	12.85	
17	474.51	1624.44	E_g
18	473.56	1621.80	E_g
19	446.94	0.34	
20	446.28	0.13	
21	446.11	0.30	
22	437.62	0.36	
23	436.67	0.23	
24	436.43	0.29	
25	427.16	0.80	
26	424.92	0.45	
27	424.73	0.88	
28	291.40	0.06	
29	291.36	0.14	
30	290.74	0.01	
31	234.20	0.04	
32	233.72	0.07	
33	232.70	0.12	
34	40.91	82.26	
35	23.60	8.69	
36	8.02	30.30	

Table S6: Calculated vibrational modes of the NiOOH bulk slab (Fig. 4 in the manuscript) without the acoustical modes.

mode	$\tilde{\nu}$ [cm^{-1}]	activity [a.u.]
01	2258.86	12816.01
02	2234.43	11816420.39
03	1153.07	141277.75
04	1128.37	9.40
05	1125.05	198740.92
06	1063.61	10.01
07	583.07	7.95
08	576.35	753870.83
09	543.63	4.73
10	530.02	4.85
11	522.35	2.68
12	485.83	2.61
13	457.87	368570.00
14	423.25	15.71
15	370.60	1871797.44
16	362.74	91978.25
17	334.80	6.49
18	294.34	717668.63
19	228.20	12.13
20	223.08	3.68
21	131.34	1061183.26

Table S7: Vibrational modes of NiOOH surface slab.

mode	$\tilde{\nu}$ [cm^{-1}]	activity [a.u.]
01	3730.18	6631094257
02	3728.59	9154490
03	2289.13	4961035920
04	2272.63	152717392414
05	1160.95	399001126
06	1108.64	15554101455
07	1076.20	11299753275
08	1073.82	781277056
09	761.48	69115440
10	646.98	365005500
11	585.06	304222811
12	571.6	1096963089
13	569.04	73917148
14	567.44	213522743
15	559.84	321699023
16	550.40	665004090
17	543.42	117369476
18	538.94	154363111
19	528.95	4669896
20	523.00	72064442
21	511.89	233511837
22	495.53	13732920
23	491.30	233300625
24	480.05	409791104
25	452.29	636332291
26	445.75	1214547250
27	400.95	642857652
28	380.26	2050023014
29	379.93	1423877648
30	376.84	2714613947
31	370.33	49380784
32	359.96	439201875
33	352.48	448541519
34	347.30	310210880
35	325.46	44661909
36	297.22	37336459
37	255.85	1813886264
38	244.11	33127693
39	228.67	4794217
40	222.33	28245980

Table S8: Vibrational modes of NiOOH surface (continuation).

mode	$\tilde{\nu}$ [cm^{-1}]	activity [a.u.]
41	211.86	48032700
42	198.73	114201700
43	197.44	385420189
44	188.23	11727270
45	102.00	112458954221
46	93.67	5535636871
47	45.55	254677279
48	39.93	929892279

References

(1) Trotochaud, L.; Young, S. L.; Ranney, J. K.; Boettcher, S. W. Nickel–Iron Oxyhydroxide Oxygen-Evolution Electrocatalysts: The Role of Intentional and Incidental Iron Incorporation. *Journal of the American Chemical Society* **2014**, *136*, 6744–6753.

(2) Diaz-Morales, O.; Ferrus-Suspedra, D.; M. Koper, M. T. The Importance of Nickel Oxyhydroxide Deprotonation on Its Activity towards Electrochemical Water Oxidation. *Chemical Science* **2016**, *7*, 2639–2645.

(3) Gao, P.; Gosztola, D.; Leung, L.-W. H.; Weaver, M. J. Surface-Enhanced Raman Scattering at Gold Electrodes: Dependence on Electrochemical Pretreatment Conditions and Comparisons with Silver. *Journal of Electroanalytical Chemistry and Interfacial Electrochemistry* **1987**, *233*, 211–222.

(4) Yeo, B. S.; Bell, A. T. In Situ Raman Study of Nickel Oxide and Gold-Supported Nickel Oxide Catalysts for the Electrochemical Evolution of Oxygen. *The Journal of Physical Chemistry C* **2012**, *116*, 8394–8400.

(5) Eilers, P. H.; Boelens, H. F. Baseline Correction with Asymmetric Least Squares Smoothing. *Leiden University Medical Centre Report* **2005**, *1*, 5.

(6) Savitzky, Abraham.; Golay, M. J. E. Smoothing and Differentiation of Data by Simplified Least Squares Procedures. *Analytical Chemistry* **1964**, *36*, 1627–1639.

(7) Newville, M.; Otten, R.; Nelson, A.; Stensitzki, T.; Ingargiola, A.; Allan, D.; Fox, A.; Carter, F.; Rawlik, M. LMFIT: Non-Linear Least-Squares Minimization and Curve-Fitting for Python. Zenodo, 2025.

(8) Kresse, G.; Furthmüller, J. Efficiency of Ab-Initio Total Energy Calculations for Metals and Semiconductors Using a Plane-Wave Basis Set. *Computational Materials Science* **1996**, *6*, 15–50.

(9) Kresse, G.; Furthmüller, J. Efficient Iterative Schemes for Ab Initio Total-Energy Calculations Using a Plane-Wave Basis Set. *Physical Review B* **1996**, *54*, 11169–11186.

(10) Blöchl, P. E. Projector Augmented-Wave Method. *Physical Review B* **1994**, *50*, 17953–

17979.

(11) Perdew, J. P.; Burke, K.; Ernzerhof, M. Generalized Gradient Approximation Made Simple. *Physical Review Letters* **1996**, *77*, 3865–3868.

(12) Zaffran, J.; Caspary Toroker, M. Benchmarking Density Functional Theory Based Methods To Model NiOOH Material Properties: Hubbard and van Der Waals Corrections vs Hybrid Functionals. *Journal of Chemical Theory and Computation* **2016**, *12*, 3807–3812.

(13) Grimme, S.; Antony, J.; Ehrlich, S.; Krieg, H. A Consistent and Accurate Ab Initio Parametrization of Density Functional Dispersion Correction (DFT-D) for the 94 Elements H-Pu. *The Journal of Chemical Physics* **2010**, *132*, 154104.

(14) Monkhorst, H. J.; Pack, J. D. Special Points for Brillouin-zone Integrations. *Physical Review B* **1976**, *13*, 5188–5192.

(15) Glemser, O.; Einerhand, J. Die Struktur höherer Nickelhydroxyde. *Zeitschrift für anorganische Chemie* **1950**, *261*, 43–51.

(16) Martirez, J. M. P.; Carter, E. A. Effects of the Aqueous Environment on the Stability and Chemistry of β-NiOOH Surfaces. *Chemistry of Materials* **2018**, *30*, 5205–5219.

(17) Fonari, A.; Stauffer, S. Raman-Sc/VASP. raman-sc, 2013.

(18) Porezag, D.; Pederson, M. R. Infrared Intensities and Raman-scattering Activities within Density-Functional Theory. *Physical Review B* **1996**, *54*, 7830–7836.

(19) Li, L.-F.; Li, Y.-F.; Liu, Z.-P. Oxygen Evolution Activity on NiOOH Catalysts: Four-Coordinated Ni Cation as the Active Site and the Hydroperoxide Mechanism. *ACS Catalysis* **2020**, *10*, 2581–2590.

(20) Tkalych, A. J.; Yu, K.; Carter, E. A. Structural and Electronic Features of β-Ni(OH)2 and β-NiOOH from First Principles. *The Journal of Physical Chemistry C* **2015**, *119*, 24315–24322.

(21) Javad Eslamibidgoli, M.; Groß, A.; Eikerling, M. Surface Configuration and Wettability of Nickel(Oxy)Hydroxides: A First-Principles Investigation. *Physical Chemistry*

Chemical Physics **2017**, *19*, 22659–22669.

(22) He, Z.-D.; Tesch, R.; Eslamibidgoli, M. J.; Eikerling, M. H.; Kowalski, P. M. Low-Spin State of Fe in Fe-doped NiOOH Electrocatalysts. *Nature Communications* **2023**, *14*, 3498.

(23) Conesa, J. C. Electronic Structure of the (Undoped and Fe-Doped) NiOOH O2 Evolution Electrocatalyst. *The Journal of Physical Chemistry C* **2016**, *120*, 18999–19010.

(24) Hu, Q.; Xue, Y.; Kang, J.; Scivetti, I.; Teobaldi, G.; Selloni, A.; Guo, L.; Liu, L.-M. Structure and Oxygen Evolution Activity of β-NiOOH: Where Are the Protons? *ACS Catalysis* **2022**, *12*, 295–304.